EARTHQUAKE ENGINEERING AND STRUCTURAL DYNAMICS
Earthquake Engng. Struct. Dyn. **28**, 1235–1254 (1999)

HIGH-FIDELITY CONTROL OF A SEISMIC SHAKE TABLE

J. KUEHN*,†, D. EPP† AND W. N. PATTEN
Center for Structural Control, University of Oklahoma, 865 Asp Ave, Room 212, Norman, OK 73019, U.S.A.

SUMMARY

A high-fidelity PC-based control system has been developed to improve the tracking characteristics of a small-scale seismic motion simulator used for testing structural control designs. This work outlines the development and testing of the control system. First, the simulator hardware is described in detail. The process of constructing a mechanistic model of the system and identifying model parameters is then described. Next, a closed-loop feedback/feed-forward control algorithm, based on an optimal receding horizon formulation, is developed. The control design was tested and the results indicate that the seismic shake table precisely tracked reference seismic motions. Copyright © 1999 John Wiley & Sons, Ltd.

KEY WORDS: hydraulic; seismic; motion simulator; shake table; receding horizon control; feed-forward control

INTRODUCTION

The civil engineering community is vigorously investigating technologies that promise to make structures and lifelines less vulnerable to the potentially ravaging vibrations that accompany and follow an earthquake. This effort includes examinations of a wide variety of engineering issues that range from the establishment of alternative specifications for the design and construction of new structures to the experimental validation of vibration absorbing hardware systems that are proposed for retrofitting existing structures.

To obtain a meaningful experimental evaluation of any proposed seismic technology, it is critical that the test procedures used guarantee the veracity of the reported results. The work reported here focuses on the design of a control strategy to ensure reliability and repeatability of test results that are obtained using a seismic shake table. Experimental data from seismic shake table tests should be considered suspect unless the investigator has established that the performance characteristics of the particular table used are sufficient for the tests. Shake table performance is largely governed by the adequacy of the hardware (in terms of the test loads being examined), and the fidelity with which the seismic shake table can reproduce a prescribed motion

*Correspondence to: J. Kuehn, Center for Structural Control, University of Oklahoma, 865 Asp Ave, Room 212, Norman, OK 73019-0601, U.S.A. E-mail: jkuehn@ou.edu.
†Ph.D. Candidate

CCC 0098–8847/99/111235–20$17·50

Received 11 October 1998
Revised 6 May 1999
Accepted 17 May 1999

time history. A shake table operated outside of the high-fidelity range can result in corrupted test data, making those results useless for comparison with test results obtained on a different shake table.

The purpose of this paper is to make the practitioner aware of a family of techniques and procedures that, when implemented, will ensure that the seismic shake table is operating with desired levels of performance. It will describe a direct procedure to guarantee that a shake table will deliver a dynamic input to a test specimen that closely matches a reference seismogram.

The paper includes a brief review of the literature. A description of the seismic shake table used in the work reported here is also included. The development of a reliable dynamic model of the electro-hydraulic components of the test systems is described. Next, a recipe for the automatic generation of a feedback/feedforward control system for the seismic shake table is provided. Experimental results are reported to substantiate the effectiveness of the closed-loop seismic shake table controller. The paper then examines the effectiveness of the design if the seismic shake table model is inexact, or if the test specimen introduces large reaction loads to the seismic shake table during the tests. The paper closes with a list of recommendations that, if adopted, will help provide a common means of assessing the performance of the equipment used for seismic testing.

BACKGROUND

Until recently, the few seismic shake tables in use in America were typically constructed with massive elements in order to minimize the interaction between the test specimen and the table. These simulators are extremely expensive to build and operate, and their availability for testing is limited.

A recent 5-year initiative by the US National Science Foundation has resulted in a significant increase in the number of investigators now exploring new seismic protection methods for structures. For example a great deal of effort is now underway to demonstrate the feasibility of structural control for seismic protection.[1,2]

Many of the investigators exploring seismic structural control solutions are conducting their research at institutions that are remote from the few very large shake table facilities. In order to validate their proposed designs, investigators are resorting to small (non-massive) shake tables. The utilization of small seismic shake tables by various investigators makes it imperative that attention be paid to the fidelity of the seismic shakle table to ensure the validity of any reported results.

Blondet and Esparza analytically investigated interaction effects between a seismic simulator and a single-Degree-of-Freedom (DOF) test structure.[3] The work indicated that the interaction between the simulator and test structure significantly distorted the simulator tracking response near the natural frequency of the structure. The coupling was also shown to reduce the stability margins of the simulator.

Newell *et al.* developed a Kalman-filter-based controller for the seismic simulator at the University of Notre Dame.[4] The controller utilized an optimal reference trajectory obtained by minimizing acceleration tracking error. The optimization incorporated a non-linear realization of the simulator dynamics. The non-linear system model was linearized about the reference trajectory and the resulting non-autonomous system was used to develop time-varying feedback gains. The tracking response of the control was experimentally verified using the 1934 El Centro west

earthquake as a reference. The mean position error was 0·0186 mm with a standard deviation of 0·135 mm. The experiment did not include a test structure on the shaker.

Crewe *et al.* compared the tuning characteristics of three 6-DOF seismic simulators in Europe.[5] The focus of the work was to demonstrate that virtually any seismic test could be conducted at all three facilities with identical results. The simulators utilize hardware feedback control systems and software algorithms, which iteratively tune reference inputs to minimize tracking error. Tests were conducted at each facility for a variety of earthquake inputs with a bare table, two rigid test specimens and two flexible test specimens. The results indicated that each system required a rigorous tuning effort to achieve the desired response characteristics for the flexible test structures.

Dai *et al.* utilized a symmetric tensor formulation of the non-linear regulator design to obtain a non-linear tracking controller.[6] The reference command for the controller was obtained by inverting the simulator dynamics. The control was experimentally shown to exhibit better tracking performance than a linear control design for the vertical component of the 1940 El Centro earthquake. The work did not include a test structure.

A recent ASCE Conference included sessions devoted to small-scale seismic simulators. Several researchers focused on simulator hardware design and development issues.[7–10]

Symans and Twitchell developed two linearized models for the uniaxial seismic simulator at Washington State University.[11] The first model was obtained for the bare table while the second included the dynamics of a single-storey test structure. The transfer function magnitudes of the models were shown to closely match experimental transfer function data. The results for the case including the building structure indicated a significant peak/notch in the amplitude response near the natural frequency of the building. The work did not present the phase characteristics of the simulator.

Trombetti *et al.* developed a linear model to assist in tuning control gains for the 1-DOF seismic motion simulator at Rice University.[12] The model includes actuator dynamics and servovalve delay as well as the flexibility of the reaction frame and the test structure. The model also accounts for the control system with PID, ΔP and feed-forward gains.

Spencer and Yang focused on improving the acceleration tracking of the seismic simulator at the University of Notre Dame.[13] The authors used a transfer function iteration technique to tune the reference command. The control method was shown to track a component of the El Centro earthquake with fidelity. The work did not include a test structure.

The focus of the work here was to develop a high-performance, low-cost controller to enhance the tracking performance of the seismic simulator at the University of Oklahoma. To maintain a low cost, a Personal Computer (PC) outfitted with A/D and D/A interfaces was used to implement the control algorithm. Rather than accounting for the varying dynamic characteristics of the test structure, it was desired to construct a control system that was insensitive to disturbance forces imparted by the test specimen.

SHAKE TABLE HARDWARE

The seismic simulator at the University of Oklahoma is shown in Figure 1. The assembly, depicted in Figure 2, consists of a 635 kg welded steel motion platform (A) with a 1·8 m × 1·2 m horizontal footprint. The motion of the table is constrained to a single horizontal axis with Thomson 75 mm extra rigid precision linear bearing (B). The support frame (C) is constructed

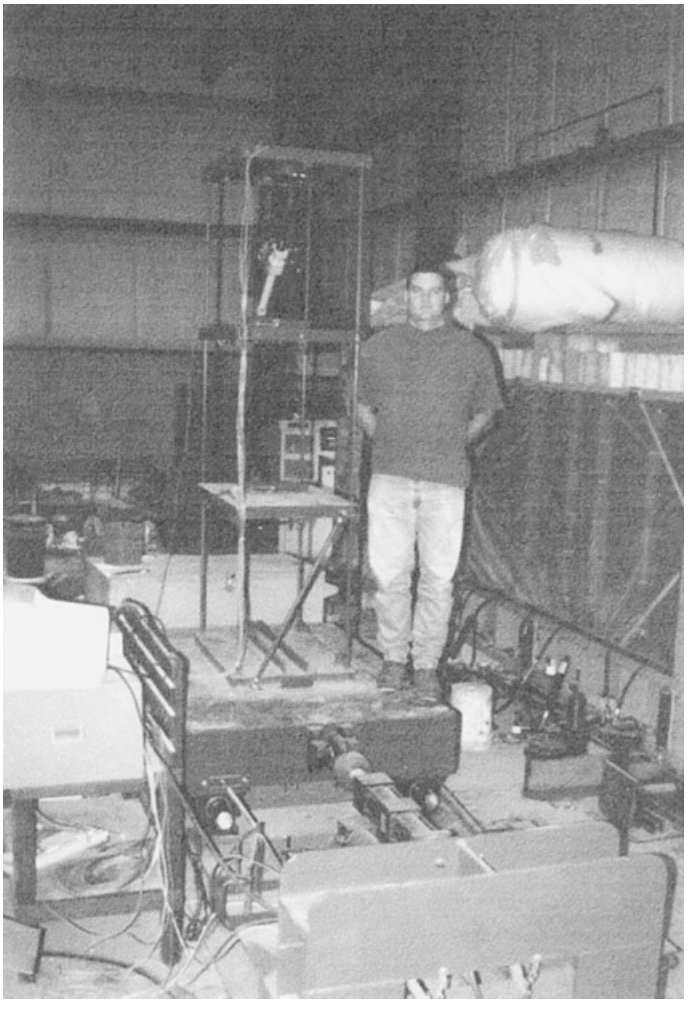

Figure 1. The seismic simulator with a test structure

from W12 × 65 wide flange I-beam and is bolted to reaction mass (D). The table is actuated with a fatigue rated 50 kN MTS hydraulic cylinder (E). The actuator has an effective piston area of $2{\cdot}5 \times 10^{-3}$ m^2 and $\pm 0{\cdot}07$ m dynamic stroke.

A schematic of the hydraulic system is provided in Figure 3. Hydraulic flow to the actuator (E) is controlled by dual MTS 252 servovalves (F). Each valve is rated to 57 lpm maximum flow at 21 MPa. The hydraulic power unit consists of a 37 kW 3-Phase AC motor that drives a Parker variable displacement piston pump (G) with a maximum flow capacity of 95 lpm at 21 MPa. The system includes 1 l hydraulic accumulators (H) mounted on both the supply and return ports of the servovalves and a 10 l accumulator (I) at the pump to stabilize the supply pressure.

The digital control system was implemented with a 200 MHz PC utilizing a Real Time Device's ADA3100 data acquisition module with 12-bit differential A/D and D/A for analog interfacing.

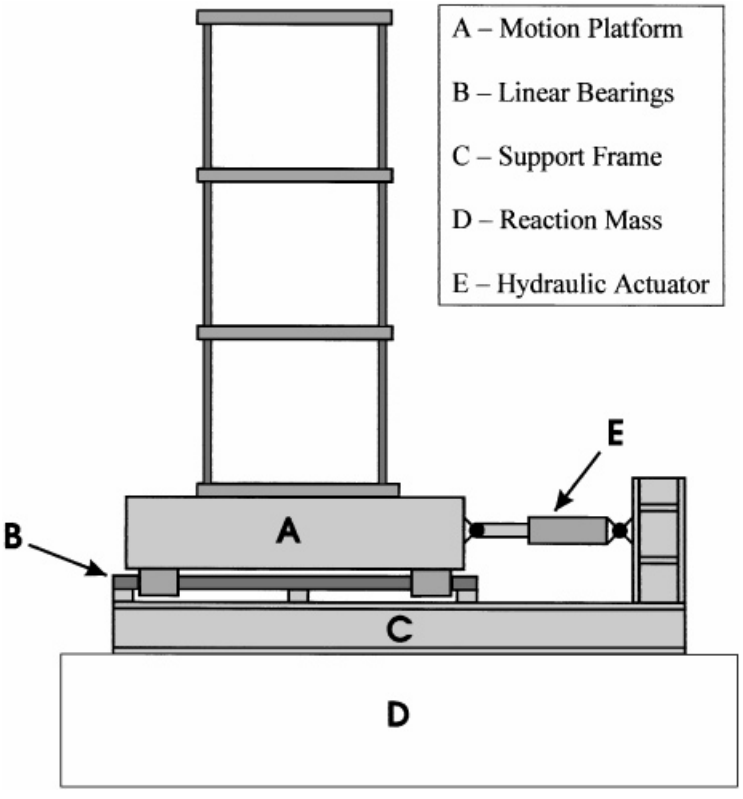

Figure 2. Seismic simulator schematic

Each A/D channel was outfitted with a second-order low-pass Butterworth filter to prevent aliasing. The break frequency of each filter was set at 500 Hz.

A variety of sensors and signal conditioning components are integrated into the simulator assembly to monitor the state of the hydraulics and the motion of the platform. The differential pressure of the actuator is sensed with an MTS differential pressure transducer. The bandwidth of the pressure sensor is DC to 1000 Hz. The platform displacement is measured with a DC/DC LVDT, manufactured by RDP Electrosense, which has a bandwidth of 0–200 Hz. Accelerations on the table and the test structure are sensed with ICS model 3028-002 piezo-resistive accelerometers. The accelerometers provide flat frequency response from DC to 1 kHz.

SYSTEM DYNAMICS

The analyst, faced with the challenge of developing a control design, must first establish a causal relationship between the input to the seismic shake table and it's output response. There are two general approaches that are used to accomplish that task; 'Black Box' identification or model synthesis based on the physics of the process. Either process will suffice if the system behaves in a linear fashion about a set operating point. The drawback to a Black Box approach is that the

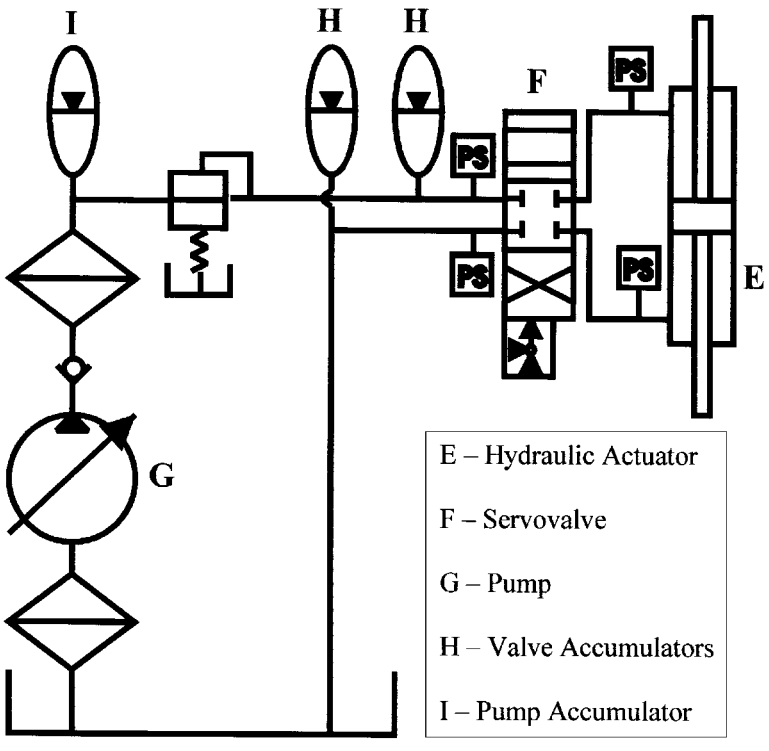

Figure 3. Hydraulic schematic

model produced by the technique provides no insight into the dynamic process variables. The Black Box approach masks opportunities to improve open-loop performance which is often an efficient first step in designing a system that is a candidate for closed-loop regulation. The following paragraphs outline the most significant features of the development of a physical model for a single degree of freedom seismic shake table. That model provides a rational basis for the design of a feedback controller in a later section.

The equation of motion for the seismic shake table platform is

$$M\ddot{x} = A_P \Delta P - C\dot{x} + f + d \tag{1}$$

where M is the platform mass, x is the horizontal displacement of the platform, A_P is the effective piston area, ΔP is the differential pressure between the actuator chambers, C is the viscous damping coefficient, f is the net friction force acting on the system and d is the net disturbance force applied to the table.

The hydraulic actuator can be characterized by neglecting leakage and applying the continuity equation to each chamber, resulting in

$$\begin{aligned} Q_1 &= \frac{\mathrm{d}V_1}{\mathrm{d}t} + \frac{V_1}{\beta_{1e}} \frac{\mathrm{d}P_1}{\mathrm{d}t} \\ -Q_2 &= \frac{\mathrm{d}V_2}{\mathrm{d}t} + \frac{V_2}{\beta_{2e}} \frac{\mathrm{d}P_2}{\mathrm{d}t} \end{aligned} \tag{2}$$

where Q_1 is the flow into chamber 1, Q_2 is the flow out of the chamber 2, V_1 and V_2 are the volumes of chambers 1 and 2 in the cylinder, β_{1e} and β_{2e} are the effective bulk moduli in the two chambers, and P_1 and P_2 are the pressures in the two chambers. Defining the relationship between the chamber volumes and the piston position gives

$$V_1 = V_{01} + A_P x, \qquad V_2 = V_{02} - A_P x \tag{3}$$

where V_{01} and V_{02} are the constant equilibrium values for the volume in each chamber, x is the position of the piston, and A_P is the effective piston area. Differentiating equation (3) yields the relations between velocity and change in volume

$$\frac{dV_1}{dt} = A_P \dot{x}, \qquad \frac{dV_2}{dt} = -A_P \dot{x} \tag{4}$$

By defining the load flow as

$$Q_L = \frac{Q_1 + Q_2}{2} \tag{5}$$

equations (2), (4) and (5) are combined to yield

$$Q_L = A_P \dot{x} + \frac{V_1}{2\beta_{1e}} \frac{dP_1}{dt} - \frac{V_2}{2\beta_{2e}} \frac{dP_2}{dt} \tag{6}$$

Assuming the bulk moduli are the same for both chambers and the actuator piston only makes small displacements about mid-stroke, equation (6) can be approximated as

$$Q_L = A_P \dot{x} + \frac{V_T}{4\beta} \Delta \dot{P} \tag{7}$$

where β is the effective bulk modulus of the hydraulic fluid and V_T is the total volume of the two chambers. The assumption that the piston only makes small displacements about mid-stroke is not necessarily valid for large amplitude motions, in this case earthquake trajectories. The assumption can be justified if the control system exhibits sufficient performance in the presence of such modelling errors. However, if the desired performance levels cannot be attained, it may be necessary to linearize equation (6) about the reference trajectory to obtain a time-varying realization of the hydraulics. Similarly, by neglecting leakage and assuming that the return pressure is small and the valve is ideal, symmetric, and matched, the equation for the load flow through the valve can be expressed as

$$Q_L = C_d |A_v| \frac{x_s}{|x_s|} \sqrt{\frac{1}{\rho}\left(P_s - \frac{x_s}{|x_s|}\Delta P\right)} \tag{8}$$

where C_d is the discharge coefficient of the valve, A_v is the valve area, x_s is the valve spool position, ρ is the hydraulic fluid density, and P_s is the supply pressure.[14] Equation (8) can be linearized using a first-order Taylor expansion to obtain

$$Q_L = K_Q x_s + K_C \Delta P \tag{9}$$

where K_Q is the flow gain, and K_C is the flow pressure coefficient. Combining equations (7) and (9) results in a linear hydraulic model

$$\frac{V_t}{4\beta}\Delta\dot{P} + A_P\dot{x}_P = K_Q x_s + K_C\Delta P \tag{10}$$

An experimental procedure was used to establish a first-order lag model of the dynamics of the two-stage valve

$$\dot{x}_s + \omega x_s = K_V u \tag{11}$$

where ω is the natural frequency of the valve spool, K_V is the servovalve gain, and u is the control voltage.

If the friction and disturbance forces are neglected, then the resulting state space model becomes

$$\dot{\hat{x}} = A\hat{x} + Bu \tag{12}$$

where

$$\dot{x} = [x \quad \dot{x} \quad \Delta P \quad x_s]^T \tag{13}$$

The measured outputs of the system are x and ΔP.

The open-loop system frequency response was measured using a Tektronics 2642a analyzer. The system was excited with 1–100 Hz random 0·1, 0·2, 0·3, and 0·4 V RMS reference inputs. The system model parameters were identified with a trial and error method and a sensitivity analysis to match the nominal experimental and analytical transfer function curves. The experimental

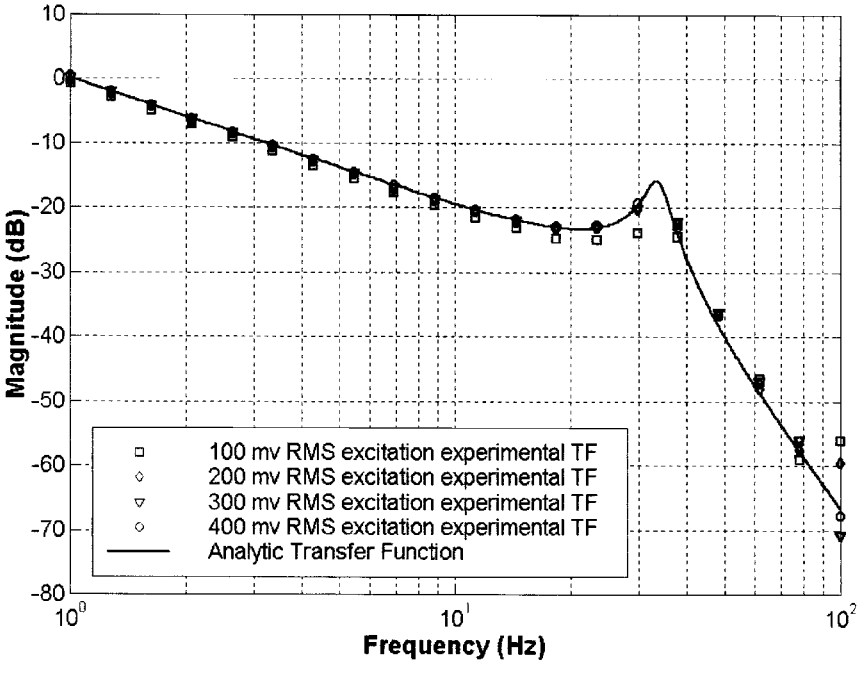

Figure 4. Comparison of the experimental and analytical magnitude transfer functions for position verses input

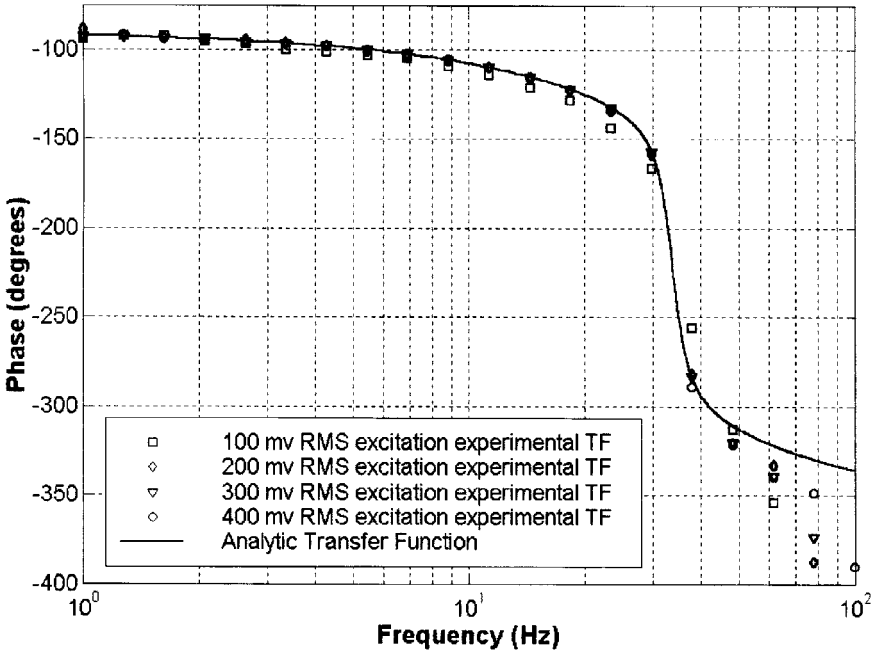

Figure 5. Comparison of the experimental and analytical phase transfer functions for position verses input

open-loop transfer function for x/u and $\Delta P/u$ are compared to the final dynamic model of the system in Figures 4–7. The resulting system matrices obtained from the identification process are provided in Appendix 1.

CONTROL DESIGN

The objective of the seismic simulator is to reproduce reference seismic motion inputs with minimal distortion in spite of modeling errors and regardless of the dynamic influence of the test specimen. The particular design approach used below produces a nearly perfect matching of the amplitude and phase components of the output versus command transfer function. The controller also provides significant disturbance rejection, thus minimizing the adverse effects that occur when the dynamics of the test structure couple with the dynamics of the shaker mechanism. The method utilizes the classical optimal regulation formulation to characterize the control design objective.[15]

$$\text{Minimize } J[\hat{x}, \hat{r}, u] \tag{14}$$

where

$$J = \frac{1}{2}\int_{t_i}^{t_i+T_H} [[\hat{x}(t) - \hat{r}(t)]^T Q[\hat{x}(t) - \hat{r}(t)] + [u(t)]^T Ru(t)]\,dt \tag{15}$$

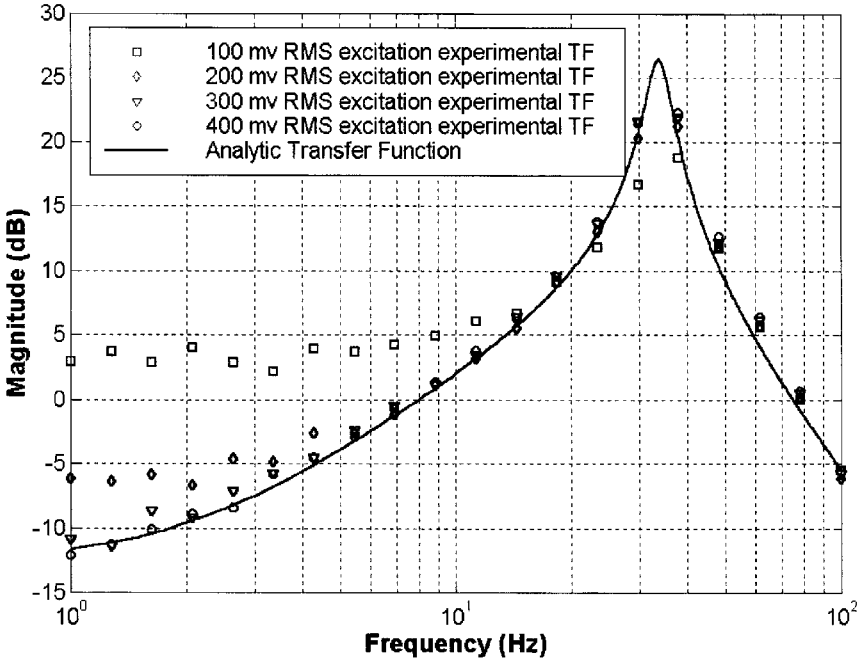

Figure 6. Comparison of the experimental and analytical magnitude transfer functions for differential pressure verses input

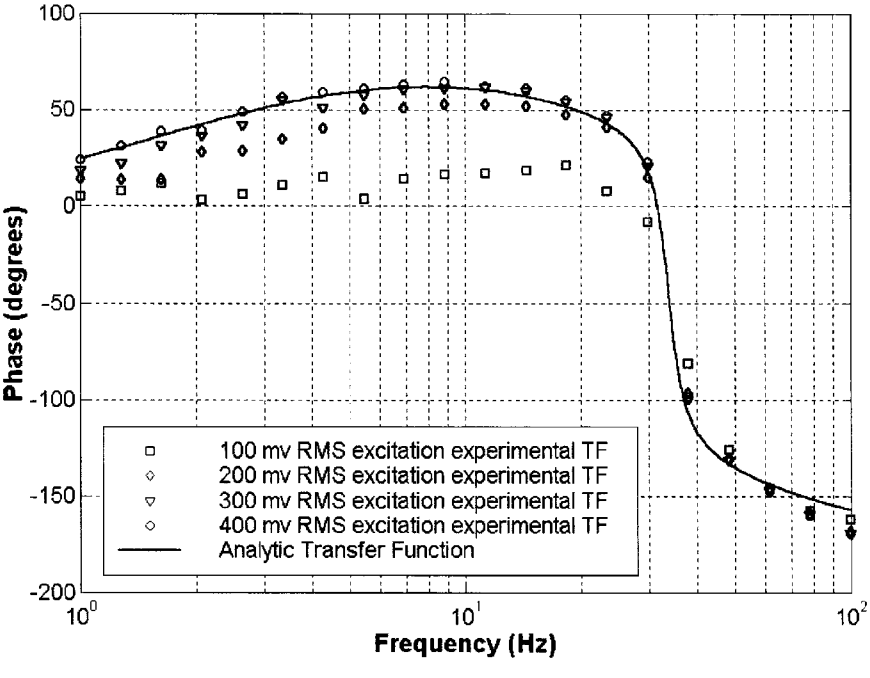

Figure 7. Comparison of the experimental and analytical phase transfer functions for differential pressure verses input

subject to equation (12) and the initial condition $\hat{x}(t_i)$. T_H is a finite horizon length, $\hat{r}$ is the reference trajectory, Q is a positive semi-definite penalty matrix on the state error, and R is a positive-definite penalty on the control input. For a fixed upper limit, it is easy to show that the derivation produces an algebraic mapping between the initial conditions, the required trajectory and the optimal control at each instant. The computation of the matrices and vectors that characterize the solution can be formidable, and it is unlikely that they could be computed in real time. In order to avoid that difficulty, the computations are carried out once (off-line), and the problem is repeated after each interval of time without changing the interval of the integration. The procedure is referred to as receding horizon control (RHC).[16,17] The algebraic result yields a two-component control law

$$u(t_i) = u_{FB} + u_{FF} \tag{16}$$

The term u_{FB} represents the feedback control,

$$u_{FB} = K_{FB}\hat{x}(t_i) \tag{17}$$

and u_{FF} is the feed-forward correction to the control

$$u_{FF} = K_{FF}\hat{r}_i^* \tag{18}$$

where

$$\hat{r}_i^* = [\hat{r}_i \quad \hat{r}_{i+1} \cdots \hat{r}_{i+n}] \tag{19}$$

The subscript i is indicative of the current time step. Because the receding horizon method is used, the gain matrices K_{FB} and K_{FF} are time invariant. A complete development of the necessary conditions produced by the control problem and the solution of those conditions is provided in Appendix II. At each update, a new control value $u(t_i)$ is computed using the current value of the state $\hat{x}(t_i)$ and the updated trajectory command vector $\hat{r}$. The control is assumed to be constant over the update interval (a zero-order hold). At the end of the interval, a new control is computed using an updated value of the state and a new window of the desired trajectory. The process is repeatable in real time because the RHC produces a fixed feedback gain matrix K_{FB} and a fixed feed-forward gain matrix K_{FF}.

The values of Q, R and T_H were determined by trial and error based on simulated system performance using a white noise reference input with differing levels of amplitude ranging from 0·1 to 0·4 g RMS. This approach guaranteed an unbiased design. The parameters were adjusted to minimize peak and RMS acceleration tracking errors. The tuning assumed that Q and R were constant over the horizon. Work conducted by Shen suggests that it is possible to attain additional bandwidth by varying Q over the horizon.[18] The work here did not pursue that avenue.

The preceding analysis assumes a complete knowledge of the state variables. It was pointed out above that only the position and the differential pressure were measured. It was therefore necessary to construct an estimator to obtain approximations of the unmeasured states. Defining $\tilde{x}$ as the state estimate based on the outputs $\hat{y}$ and the output matrix C, the dynamics of the observer are characterized as

$$\dot{\tilde{x}} = (A - LC)\tilde{x} + Bu + L\hat{y} \tag{20}$$

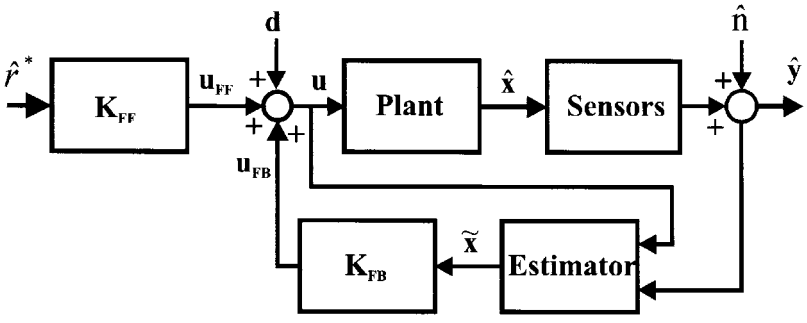

Figure 8. Block diagram of the control structure

where

$$C = \begin{bmatrix} 1 & 0 & 0 & 0 \\ 0 & 0 & 1 & 0 \end{bmatrix} \tag{21}$$

The matrix L is selected to yield a reliable estimate of the state based on the outputs and control input. The estimator design neglects any noise or disturbance. Noise can be neglected because the observed signal-to-noise ratio for the experimental setup was 40 dB. The omission of the disturbance from the estimator model can be problematic. However, if the disturbance dynamics are band limited, then it is possible to create a controller/estimator pair that essentially attenuates the effects of the disturbance, suggesting that the disturbance is negligible when estimating the state from the outputs. That is precisely the nature of the shake table problem for which the disturbance inputs reflect the modal dynamics of the structure attached to the table. The robustness of the controller/estimator pair to the disturbances is verified in a later section. The estimator was designed using the pole placement method.[19] The value of L is given in Appendix I, and the control system structure including the estimator is depicted in Figure 8.

The stability margins of the control design for the nominal system and for a system with a 100 per cent increase in the table mass are depicted in Figure 9. The open-loop simulation includes the dynamics of the estimator. The results indicate that the system is robust to significant mass changes, which would include the addition of a test structure. In both cases the gain margin was infinite and the phase margin was approximately 60°.

EXPERIMENTAL RESULTS

Once a suitable set of penalties (Q, R, T_F) were selected by iterative tuning, the effectiveness of the controller design was tested experimentally. In order to compare the performance of the RHC, a similar feedback only controller was employed. Based on the classic Linear Quadratic Regulator (LQR) design

$$J = \int_0^\infty (\hat{x}(t)^T Q \hat{x}(t) + u(t)^T R u(t))\,dt \tag{22}$$

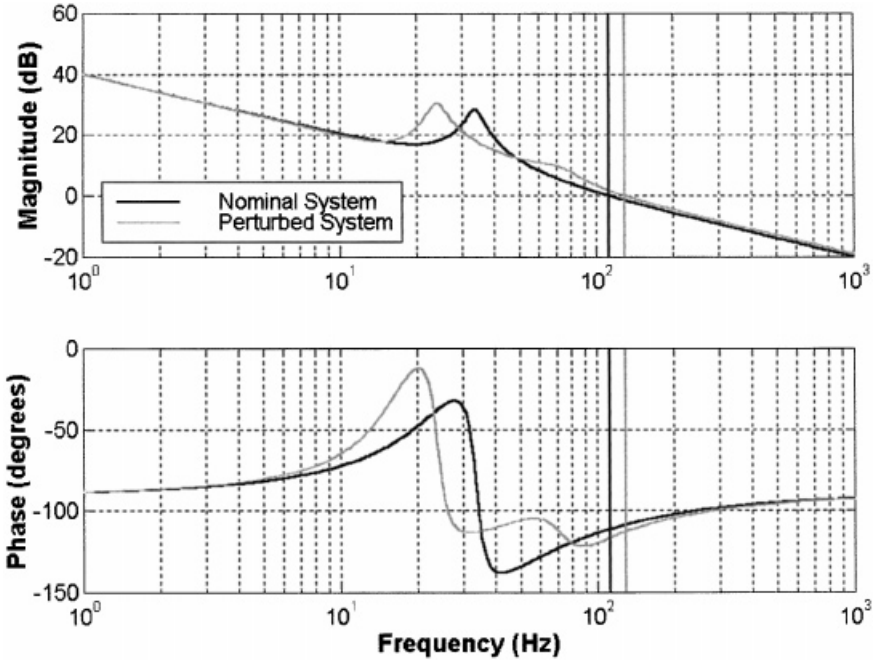

Figure 9. Open-loop displacement characteristic gain transfer function for the nominal system and for the perturbed system

subject to the system dynamics (12). The design produces a fixed feedback gain set that is used to construct a control rule

$$u(t) = K_{\mathrm{LQ}}(\hat{r}(t) - \hat{x}(t)) \tag{23}$$

The penalties Q and R used in the LQR design match those used in the RHC design.

Both the LQR and the RHC controllers were implemented with a 2 kHz update rate. The tracking performance of both designs was tested using 0·1 g RMS white noise acceleration with a 0·5–50 Hz bandwidth as a reference input. The experimentally measured transfer functions are plotted in Figures 10 and 11. Figure 10 illustrates that the amplitude responses of both controllers are flat through 40 Hz. Figure 11 indicates that a significant difference in phase characteristics exists between the two controllers. The feed-forward RHC controller compensates for the inherent phase lag of the hardware to accomplish high-fidelity tracking of all the frequency components of a command signal through 40 Hz. The LQR design, on the other hand, produces a significant distortion of any command with frequency content over 10 Hz.

The simulator's performance must also be robust to large forces imparted by flexible test structures. The experimentally measured sensitivity of the table acceleration to disturbance inputs is plotted in Figure 12. Provided the disturbances are band limited to 10 Hz, the control provides -30 dB attenuation, which confirms the decision to disregard the disturbance when designing the state estimator. In order to verify the tracking robustness of the design, two tests were conducted; one with no load on the simulator and a second with a three-storey 340 kg test

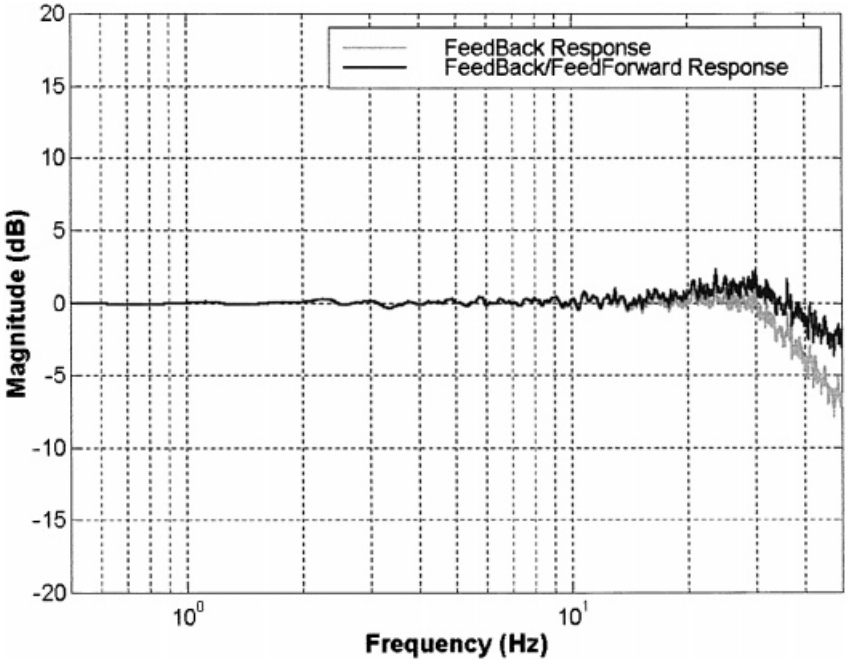

Figure 10. Magnitude transfer function comparison of LQR and FB/FF controllers

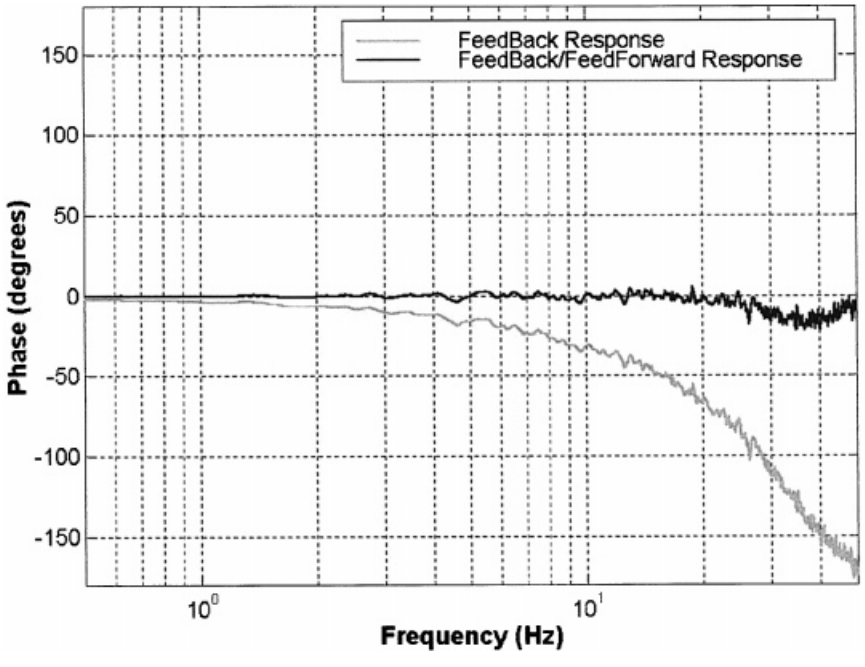

Figure 11. Phase transfer function comparison of LQR and FB/FF controllers

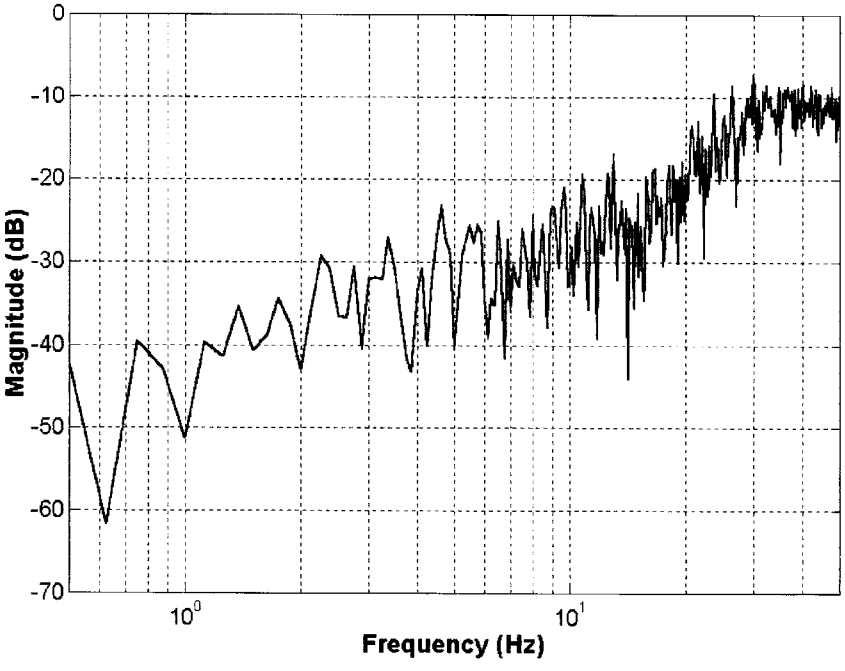

Figure 12. Sensitivity of the acceleration to disturbances

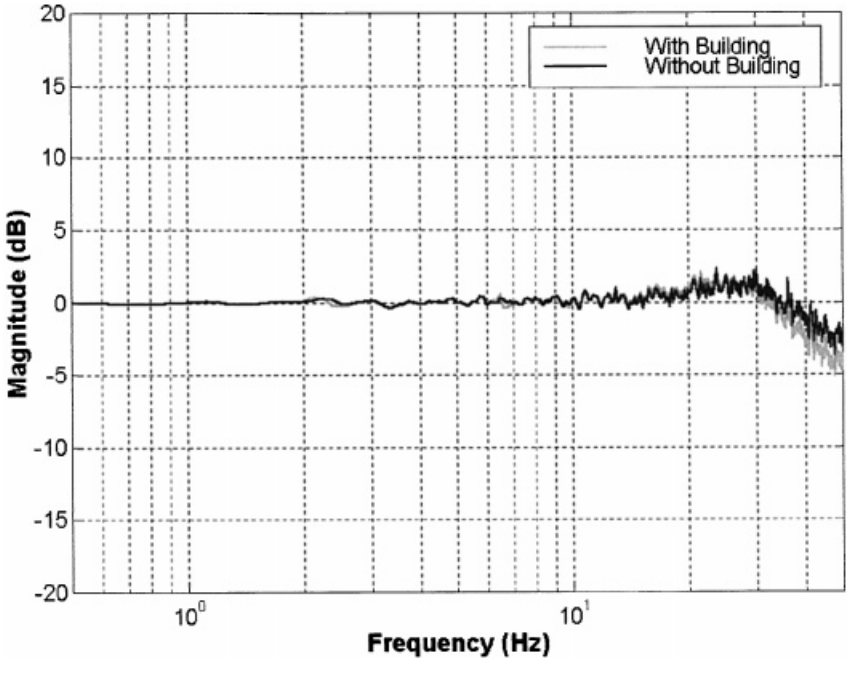

Figure 13. Magnitude transfer function comparison of FB/FF control with and without a 340 kg test structure

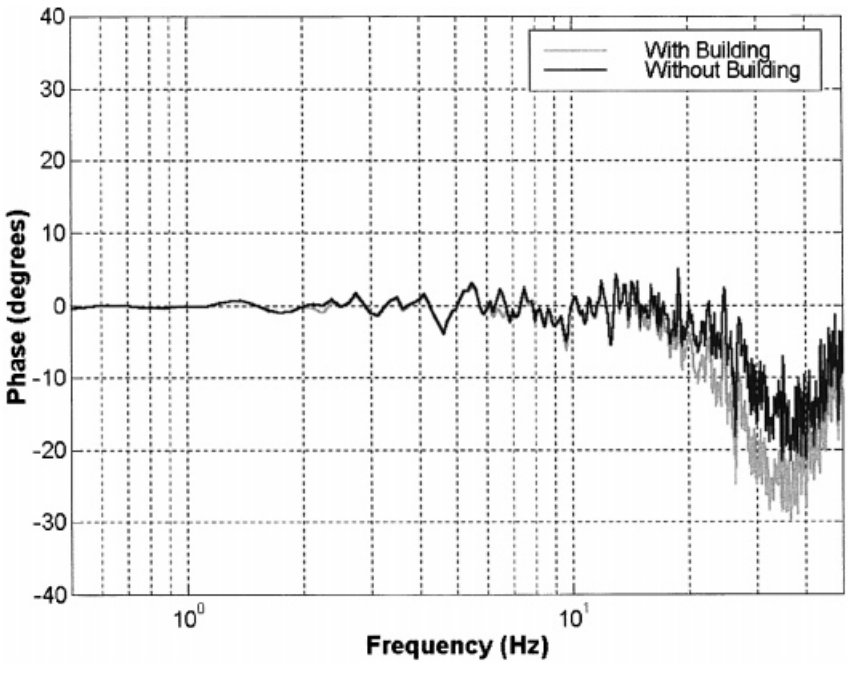

Figure 14. Phase transfer function comparison of FB/FF control with and without a 340 kg test structure

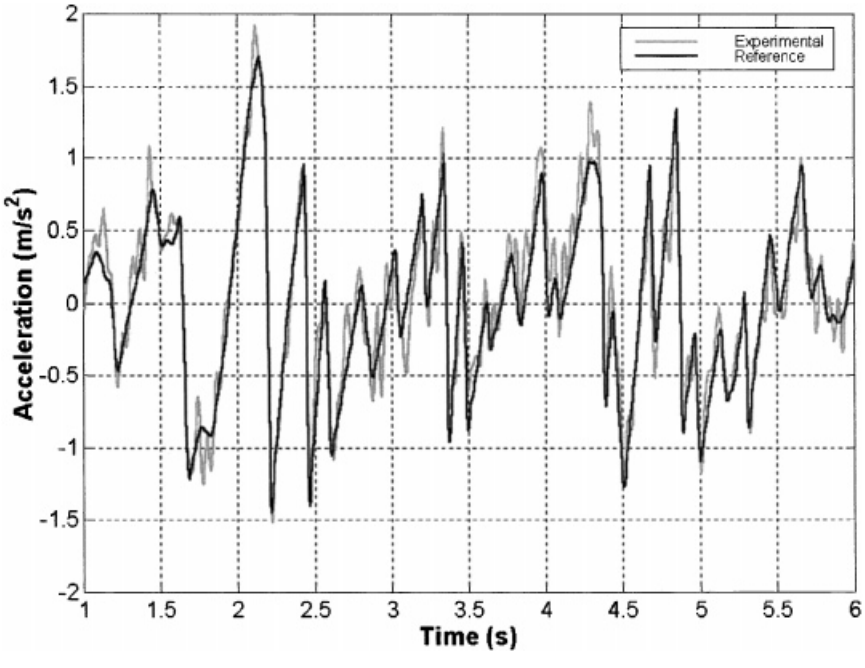

Figure 15. Time domain plot of reference acceleration (North–south component of El centro 1940 at half-scale) versus actual simulator acceleration with three-storey test structure attached

structure. The structure had natural frequencies at 2·3, 6·5 and 9·6 Hz. The 0·1 g RMS white noise input was again used as the reference trajectory for the feed-forward control algorithm. The corresponding acceleration transfer functions with and without the test specimen are compared in Figures 13 and 14. The results indicate that the additional dynamics have no discernable effect on the amplitude response performance of the system and produces a small 3 degree variation in the phase response near the natural frequencies of the test structure. A time plot of the simulator acceleration response with the test structure affixed is compared to the desired acceleration in Figure 15.

CONCLUSIONS

A high-fidelity, PC-based control system was developed for a single DOF electrohydraulic seismic shake table and the simulator hardware was described in detail. A linear approximation of the system dynamics was used to develop a control design model. A feedback/feed-forward tracking control strategy was developed using the linearized system model and was implemented with inexpensive PC control hardware. The performance of the control was experimentally tested and compared to a traditional LQR controller, and it was shown that the feedback/feed-forward control had significantly better phase characteristics than the LQR control. The performance of the control design was also shown to be insensitive to dynamic loading imparted by a three-storey test structure. If, on the other hand, the configuration of the particular table and test specimen were such that the disturbance rejection was insufficient, the designers would have to resort to the construction of a suitable representation of the dynamics of the disturbance and use that estimate to modify the conclusions of the RHC. This process would produce a second fixed feed-forward gain set. The estimated disturbance should also be injected into the state observer to produce the estimated state vector. Finally, the use of a Kalman filter is recommended as a means of further mitigating any sensor noise effects.[20]

ACKNOWLEDGEMENTS

The authors would like to thank Benjamin Wallace, Ph.D., Mike Schmitz, and Greg Brock. Their assistance was greatly appreciated during the experimental phase of this work.

REFERENCES

1. S. Dyke, B. Spencer, P. Quast and M. Sain, 'Role of control-structure interaction in protective system design', *J. Engng. Mech.* **121**(2), 322–338 (1995).
2. M. Symans and M. Constantinou, 'Seismic testing of a building structure with a semi-active fluid damper control system', *Earthquake Engng. Struct. Dyn.* **26**, 759–777 (1997).
3. M. Blondet and C. Esparza, 'Analysis of shaking table-structure interaction effects during seismic simulation tests', *Earthquake Engng. Struct. Dyn.* **16**, 473–490 (1988).
4. D. Newell, H. Dai, M. Sain, P. Quast and B. Spencer, 'Nonlinear modeling and control of a hydraulic seismic simulator', *Proc. American Controls Conf.*, Seattle, WA, 1995, pp. 801–805.
5. A. Crewe, C. Taylor, H. Mouzakis, E. Vougioukas and G. Franchioni, 'The performance of the shaking table control systems at the National Technical University of Athens, Bristol University and ISMES, Italy', *10th Int. Seminor on Earthquake Prognostics*, Cairo, 1996.
6. H. Dai, M. Sain and B. Spencer, 'Using tensors to track earthquakes of hydraulic shaker tables', *Proc. American Controls Conf.* Albuquerque, NM, 1–5, 1997.

7. M. Abdullah, K. Hu, P. Kirmser and S. Swartz, 'The KSU shaking table and the stiffness decoupler technology', *Proc. 12th Engineering Mechanics Conf.*, American Society of Civil Engineers, Reston, VA, 1998, pp. 774–778.
8. S. Dyke, 'Design and development of the Washington University Seismic Simulator facility', *Proc. 12th Engineering Mechanics Conf.*, American Society of Civil Engineers, Reston, VA, 1998, pp. 762–765.
9. S. Nagarajaiah and E. Gozdowski, 'Unidirectional shaking table for testing small scale structural models: design and development', *Proc. 12th Engineering Mechanics Conf.*, American Society of Civil Engineers, Reston, VA, 1998, pp. 779–782.
10. H. Gavin, H. Jamieson and D. Batt, 'A shaking table for experimental dynamics and control', *Proc. 12th Engineering Mechanics Conf.*, American Society of Civil Engineers, Reston, VA, 1998, pp. 787–790.
11. M. Symans and B. Twitchell, 'System identification of a uniaxial seismic simulator', *Proc. 12th Engineering Mechanics Conf.*, American Society of Civil Engineers, Reston, VA, 1998, pp. 758–761.
12. T. Trombetti, J. Conte and A. Durrani, 'Actuator-foundation-specimen interaction in a small shaking table', *Proc. 12th Engineering Mechanics Conf.*, American Society of Civil Engineers, Reston, VA, 1998, pp. 770–773.
13. B. Spencer and G. Yang, 'Earthquake simulator control by transfer function iteration', *Proc. 12th Engineering Mechanics Conf.*, American Society of Civil Engineers, Reston, VA, 1998, pp. 766–769.
14. H. Merritt, *Hydraulic Control Systems*, Wiley, New York, 1967.
15. D. Kirk, *Optimal Control Theory: An Introduction*, Prentice-Hall, Englewood Cliffs, NJ, 1970.
16. W. Kwon and D. Byun, 'Receding horizon tracking control as a predictive control and its stability properties', *Int. J. Control* **50**(5), 1807–1824 (1989).
17. P. Dorato, C. Abdallah and V. Cerone, *Linear Quadratic Control: An Introduction*, Prentice-Hall, Englewood Cliffs, NJ, 1995.
18. K. Shen, 'Model-based predictive control: tracking performance, robustness, and its application to a 3-DOF motion simulator', Thesis, presented to University of Oklahoma at Norman, OK, in partial fulfillment of the requirements for the degree of Doctor of Philosophy, 1996.
19. W. Brogan, *Modern Control Theory*, Prentice-Hall, Upper Saddle River, NJ, 1991.
20. R. Skelton, *Dynamic Systems Control*, Wiley, New York, 1988.

APPENDIX I

The experimentally identified state space model matrices are

$$A = \begin{bmatrix} 0 & 1 & 0 & 0 \\ 0 & -12{\cdot}6 & 344{\cdot}6 & 0 \\ 0 & -130{\cdot}3 & -17{\cdot}2 & 837{\cdot}7 \\ 0 & 0 & 0 & -238{\cdot}8 \end{bmatrix} \tag{24}$$

and

$$B = [0 \quad 0 \quad 0 \quad 238{\cdot}8]^{\mathrm{T}} \tag{25}$$

The penalty matrices used for the control designs are

$$Q = \begin{bmatrix} 10^4 & 0 & 0 & 0 \\ 0 & 0 & 0 & 0 \\ 0 & 0 & 1 & 0 \\ 0 & 0 & 0 & 1 \end{bmatrix} \tag{26}$$

$$R = [1] \tag{27}$$

$$T_{\mathrm{H}} = 0{\cdot}050\ \mathrm{s} \tag{28}$$

and

$$L = \begin{bmatrix} 997{\cdot}6 & 0{\cdot}7 \\ 144990{\cdot}0 & -1768{\cdot}9 \\ -14962{\cdot}0 & 978{\cdot}9 \\ 9821{\cdot}3 & -5{\cdot}8 \end{bmatrix} \tag{29}$$

APPENDIX II

For convenience of notation, the Hamiltonian is defined as

$$H = \tfrac{1}{2}[\hat{x}(t) - \hat{r}(t)]^{\mathrm{T}} Q[\hat{x}(t) - \hat{r}(t)] + \tfrac{1}{2}u(t)^{\mathrm{T}} R u(t) + \hat{p}(t)^{\mathrm{T}}[A\hat{x}(t) + Bu(t)] \tag{30}$$

The necessary conditions for minimization of the performance index (15) subject to the state equation (12) are[15]

$$\dot{\hat{x}}(t) = \frac{\partial H}{\partial \hat{p}} = A\hat{x}(t) + Bu(t) \tag{31}$$

$$\dot{\hat{p}}(t) = -\frac{\partial H}{\partial \hat{x}} = -Q\hat{x}(t) - A^{\mathrm{T}}\hat{p}(t) + Q\hat{r}(t) \tag{32}$$

$$0 = \frac{\partial H}{\partial u} = Ru(t) + B^{\mathrm{T}}\hat{p}(t) \tag{33}$$

with the boundary conditions

$$\hat{x}(t_i) = \hat{x}_i \tag{34}$$

$$\hat{p}(t_i + T_{\mathrm{H}}) = \hat{0} \tag{35}$$

The value of $\hat{x}_i$ is estimated from the sensed variables at time t_i.

Since by definition R^{-1} exists, equation (33) can be solved for the control input

$$u(t) = R^{-1}B^{\mathrm{T}}\hat{p}(t) \tag{36}$$

Therefore, the control input can be determined by solving for the costate $\hat{p}(t_i)$.

Equations (31), (32) and (36) can be recast in the form

$$\dot{\hat{z}}(t) = M\hat{z}(t) + N\hat{r}(t) \tag{37}$$

where

$$\hat{z} = \begin{bmatrix} \hat{x} \\ \hat{p} \end{bmatrix} \tag{38}$$

$$M = \begin{bmatrix} A & -BR^{-1}B^{\mathrm{T}} \\ -Q & -A^{\mathrm{T}} \end{bmatrix} \tag{39}$$

and

$$N = \begin{bmatrix} \bar{0} \\ Q \end{bmatrix} \tag{40}$$

The closed-form solution of equation (37), for any $t \in [t_i, t_i + T_H]$, can be expressed as

$$\hat{z}(t) = e^{M(t-t_i)}\hat{z}(t_i) + \int_{t_i}^{t} e^{M(r-\tau)}N\hat{r}(\tau)\,d\tau \tag{41}$$

The integral in equation (41) can be approximated by discretizing the horizon into intervals and applying a zero-order hold to $\hat{r}(t)$ on each interval, resulting in

$$\hat{z}_n = e^{M(t_n-t_i)}\hat{z}_i + e^{Mt_n}\sum_{j=i}^{n} M^{-1}[e^{-Mt_{j-1}} - e^{-Mt_j}]N\hat{r}_j \tag{42}$$

which can be expressed as

$$\hat{z}_n = \Phi z_i + \Psi[\hat{r}_i \quad \hat{r}_{i+1} \cdots \hat{r}_{i+n}]^T \tag{43}$$

where the real-valued functions Φ and Ψ are defined as

$$\Phi = \begin{bmatrix} \Phi_{11} & \Phi_{12} \\ \Phi_{21} & \Phi_{22} \end{bmatrix} = e^{M(t_n-t_i)} \tag{44}$$

and

$$\Psi = \begin{bmatrix} \Psi_1 \\ \Psi_2 \end{bmatrix} = e^{Mt_n}M^{-1}[(e^{-Mt_i} - e^{-Mt_{i+1}})N \cdots (e^{-Mt_{n-1}} - e^{-Mt_n})N] \tag{45}$$

Equation (43) can be substructured to yield the costate vector

$$\hat{p}_n = \Phi_{21}\hat{x}_i + \Phi_{22}\hat{p}_i + \Psi_2\hat{r}_i^* \tag{46}$$

where

$$\hat{r}_i^* = [\hat{r}_i, \hat{r}_{i+1}, \ldots, \hat{r}_{i+n}]^T \tag{47}$$

By setting $t_n = t_i + T_H$ and applying the terminal condition on the costate $\hat{p}_n = \hat{0}$ equation (46) can be solved for $\hat{p}_i$

$$\hat{p}_i = -\Phi_{22}^{-1}(\Phi_{21}\hat{x}_i + \Psi_2\hat{r}_i^*) \tag{48}$$

which can be substituted into equation (36) to obtain a control input of the form

$$u_i = K_{FB}\hat{x}_i + K_{FF}\hat{r}_i^* \tag{49}$$

where

$$K_{FB} = R^{-1}B^T\Phi_{22}^{-1}\Phi_{21} \tag{50}$$

and

$$K_{FF} = R^{-1}B^T\Phi_{22}^{-1}\Psi_2 \tag{51}$$

The values of Φ, Ψ, K_{FB}, and K_{FF} are constant and are computed off-line.

